ACS APPLIED MATERIALS & INTERFACES

Research Article

www.acsami.org

Ratiometric NanoCluster Beacon: A Label-Free and Sensitive Fluorescent DNA Detection Platform

Lei Ge, Ximei Sun, Qing Hong, and Feng Li*

College of Chemistry and Pharmaceutical Sciences, Qingdao Agricultural University, Qingdao 266109, P. R. China

Supporting Information

ABSTRACT: Although researches until now have emphasized the influence of an oligonucleotide sequence on the fluorescence of oligonucleotide-stabilized silver nanoclusters (AgNCs), this influence has been explored as a novel ratiometric fluorescent signal transduction in this work. This study builds on our original discovery of a template-transformation phenomenon, which demonstrated that the connection of a special DNA fragment (5′-CACCGCTTT-3′) with a green-emitting AgNC nucleation sequence (GNuS, 5′-TGCCTTTTGGGGACGGATA-3′) creates a red-emitting AgNC nucleation sequence (RNuS, 5′-CACCGCTTTTGCCTTTTGGGGACGGATA-3′). Attempts to expand this idea and construct elegant ratiometric NanoCluster Beacons (NCBs) for DNA sequence detection are not straightforward, and, thus, we carried out a series of investigations with the goal of understanding the mechanism of this template-transformation phenomenon. Experimental results showed that the six-nucleotide fragment (5′-CACCGC-3′) at the 5′-end of RNuS acts as a template convertor and takes full responsibility for the template transformation from GNuS to RNuS. Moreover, we found that the appropriate proximity of the convertor to GNuS also plays a significant role in the template transformation. We then show that the insights gained here for the template-transformation mechanism allow us to construct ratiometric NCBs by simply appending the convertor and the GNuS onto a rationally designed stem−loop probe. This new type of NCB emits intense red fluorescence without the addition of a target DNA and emerges as a new, bright green emission only when hybridized to its target DNA. By measuring the distinct variation in the fluorescence intensity ratios of green and red emission, this ratiometric NCB was demonstrated to sensitively detect Hepatitis-A virus gene sequences, a proof-of-concept target in this work, with good selectivity.

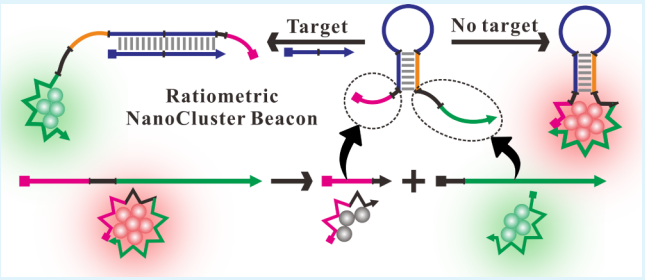

KEYWORDS: *DNA, silver nanoclusters, NanoCluster Beacons, fluorescence biosensor, ratiometric probes*

INTRODUCTION

Oligonucleotide-stabilized silver nanoclusters (AgNCs) are a significant new class of fluorescence emitters,[1,2] which are formed in aqueous environments using oligonucleotides as scaffolds and act as promising alternatives to conventional organic dyes and quantum dots. The outstanding spectral and photophysical properties,[3,4] such as high photoemission rates, excellent photostability, unobtrusive blinking, and tunable photoemission bands throughout the visible to near-infrared region from 400−900 nm, in conjunction with low cytotoxicity, high biocompatibility, ease of synthesis, and desired small size have facilitated wide and detailed exploitation of AgNCs as environmentally friendly and biocompatible fluorophores for a variety of applications, including optical sensor design for chemical/biological assay,[5−13] cellular imaging,[14−19] and information possessing.[20−22] On the basis of these attractive inherent properties, AgNCs are expected to be ideal fluorophores for designing fluorescent molecular beacons,[23−28] termed NanoCluster Beacons (NCBs), which may render further advantages over traditional fluorescence biosensors, because they are simple and inexpensive without time-consuming and complicated dual labeling of fluorophore (donor)−quencher (acceptor) pairs on the molecular beacons. However, almost all AgNC-based fluorescence biosensors have been developed on the basis of the fluorescence quenching (turn-off) or enhancing (turn-on) effects at a certain wavelength,[23−26,29−33] which generally suffer from the unavoidable disturbance induced by intensity fluctuations ascribed to, for example, the instrumental or environmental factors, resulting in degradation of the reliability of the measured results.

With this in mind, the development of accurate and sensitive ratiometric AgNC-based fluorescence biosensors, which can permit simultaneous recording of the relative fluorescence variations of two well-separated wavelengths instead of measuring single-emission-intensity changes, is in urgent demand to effectively overcome the above-mentioned concerns in the single-emission-intensity measurements. It is worth noting that ratiometric fluorescence strategies/probes[34,35] could offer a built-in environmental interference correction to permit more accurate quantification of the target concentration

Received: March 6, 2017
Accepted: April 3, 2017
Published: April 3, 2017

DOI: 10.1021/acsami.7b03198
ACS Appl. Mater. Interfaces 2017, 9, 13102−13110

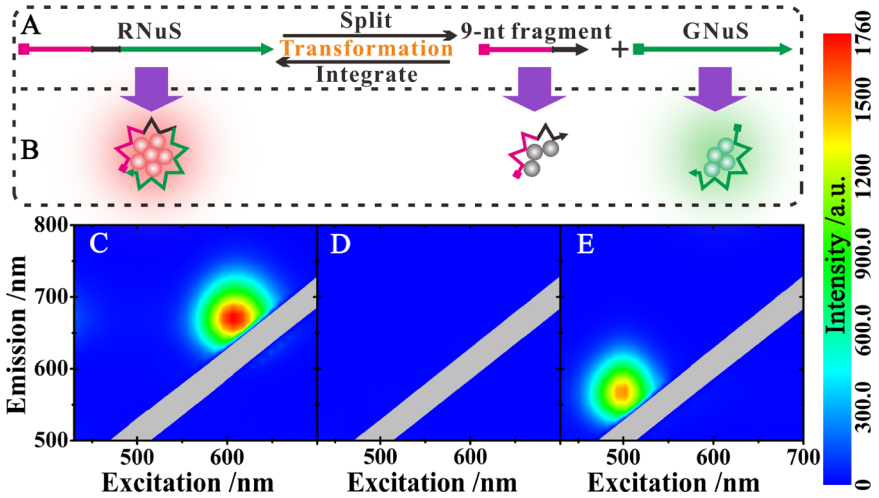

Figure 1. Schematic illustration of (A) the three DNA sequences participating in the template-transformation process and (B) their hosted AgNCs. Two-dimensional fluorescence contour maps of AgNCs stabilized by (C) RNuS, (D) 5′-CACCGCTTT-3′, and (E) GNuS. In the 2D fluorescence contour map, excitation and emission wavelengths are plotted along the horizontal and vertical axes, respectively, whereas the color indicates the detected intensity. The scattered excitation light has been subtracted and masked as gray bands (regions along $\lambda_{ex} = \lambda_{em}$). Concentrations for all sequence used in this work are 150 nM unless noted otherwise.

through eliminating systematic errors. However, until now, reports on ratiometric AgNC-based fluorescence biosensors are rare.[36] Therefore, the research in this field is still rather limited in its infancy and it is highly desirable to develop more exquisite and sensitive ratiometric AgNCs-based fluorescence biosensors. Taking these motivations into consideration and following our interest in DNA detection,[37,38] we present, herein, a novel design strategy for advanced ratiometric NCBs based on two AgNC templates exploited by Gwinn and co-workers,[39] that is, a red-emitting AgNC nucleation sequence (5′-CACCGCTTTTGCCTTTTGGGGACGGATA-3′, denoted as RNuS) and a green-emitting AgNC nucleation sequence (5′-TGCCTTTTGGGGACGGATA-3′, denoted as GNuS). As shown in Figure 1, we found that the 19-nt GNuS could be split from the 28-nt RNuS, that is, the integration of a 6-nt fragment (5′-CACCGC-3′, named as a convertor) onto the 5′ terminals of GNuS through a T_3 linker (5′-TTT-3′) would transform the GNuS to RNuS, which has not been reported or demonstrated until now.

Hence, on the basis of the observed template-transformation phenomenon, we constructed an elegant ratiometric NCB, where the convertor is attached at the 5′-end of the stem−loop probe and the GNuS is attached at the 3′-end through an appropriate T linker. In the absence of a target DNA, the ratiometric NCB adopts a hairpin structure, bringing the convertor and the GNuS into close proximity to each other, which assemble to form an intact RNuS and, upon reduction in the presence of silver ions, produce red-emissive AgNCs. When a target DNA is introduced, the NCB opens upon hybridization to its target. The disruption of the hairpin structure causes physical separation of the convertor from the GNuS, resulting in the production of green-emissive AgNCs only. In other words, this ratiometric NCB emits intense red fluorescence (peak emission at ∼670 nm) without the addition of a target DNA and emerges as a new, bright green emission (peak emission at ∼565 nm) only when it hybridizes to its target DNA. Because the percentage of the opened NCBs is directly related to the concentration of the target DNA, by measuring the distinct variation in the fluorescence intensity ratios of green and red emissions, label-free and sensitive ratiometric fluorescence sensing for the target DNA is achieved. Distinctive from the conventional molecular beacons based on energy transfer, this ratiometric NCB could be designed on the basis of the simple template-transformation strategy irrespective of the strict selection and the complicated dual-labeling of an ideal fluorophore (donor)−quencher (acceptor) pair, endowing the probes' design with more flexibility and low cost. Moreover, the significant differences of the strong emission peak wavelength between the response and background signals can avoid the interloping among the two emission peaks, and this is favorable for the development of ratiometric fluorescence nanoprobes in sensitive and accurate disease DNA detection.

EXPERIMENTAL SECTION

Chemicals and Materials. Silver nitrate ($AgNO_3$), sodium borohydride ($NaBH_4$), and sodium acetate (NaAc) were purchased from Sigma-Aldrich Chemical Co (St. Louis, MO) and used without further purification. All reagents are of analytical grade, and solutions were prepared using ultrapure water purified by a Milli-Q water purification system (Millipore Corp., Bedford, MA) with a specific resistance of 18.2 MΩ cm. All of the oligonucleotides were custom-synthesized from Sangon Biological Engineering Technology and Services Co., Ltd. (Shanghai, China). The DNA oligonucleotide sequences are listed in the Supporting Information. All of the synthetic oligonucleotides were high-performance liquid chromatography purified and freeze-dried by the supplier. They were received as powders and centrifuged so that they would reside at the bottom of the containers. The powder was then dissolved with 20 mM NaAc solution (pH 7.5) to give stock solutions of 100 μM.

Apparatus. All fluorescence emission and excitation scans were performed on an F-4600 fluorescence spectrophotometer (Hitachi Ltd., Japan) at room temperature using a quartz cuvette with a 10 mm light path. The fluorescence contour maps were collected using excitation wavelengths ranging from 430 to 700 nm, and the emission wavelengths were scanned from 500 to 800 nm. Both emission and excitation were scanned using a 10 nm slit size, a 10 nm increment step, and a 0.5 s integration time. For emission scans, the emission spectra of red-emitting AgNCs were collected from 625 to 800 nm with an excitation wavelength of 610 nm. The emission spectra of green-emitting AgNCs were collected from 520 to 800 nm with an excitation wavelength of 500 nm.

AgNC Synthesis. In this work, to study the template-transformation mechanism, different RNuS and GNuS derivatives were

DOI: 10.1021/acsami.7b03198
ACS Appl. Mater. Interfaces 2017, 9, 13102−13110

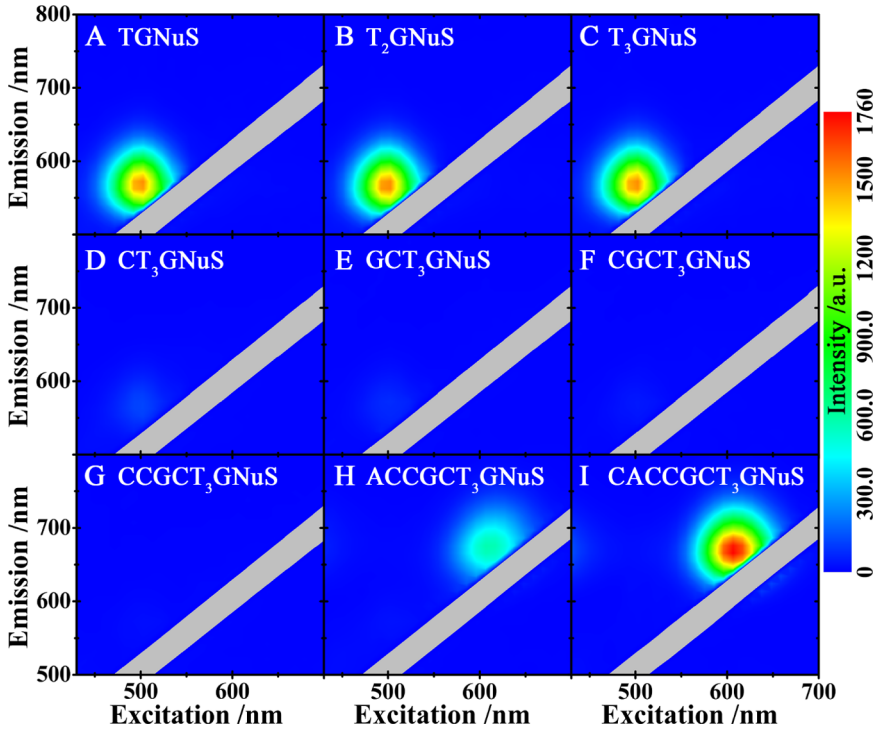

Figure 2. Two-dimensional fluorescence contour maps of AgNCs stabilized by different GNuS derivatives. (A) 5′-TGNuS-3′; (B) 5′-TTGNuS-3′; (C) 5′-TTTGNuS-3′; (D) 5′-CT_3GNuS-3′; (E) 5′-GCT_3GNuS-3′; (F) 5′-$CGCT_3$GNuS-3′; (G) 5′-$CCGCT_3$GNuS-3′; (H) 5′-$ACCGCT_3$GNuS-3′; (I) 5′-$CACCGCT_3$GNuS-3′.

used as scaffolds for AgNC synthesis, which were performed by mixing the DNA template and freshly prepared $AgNO_3$ in a NaAc solution (20 mM, pH 7.5), followed by vigorously shaking for 30 s. After incubation for 30 min in the dark at 4 °C, the obtained solutions were reduced by freshly prepared $NaBH_4$ solution with vigorously shaking for another 30 s. The final concentrations of the resultant reaction mixture were 0.15 μM DNA template, 1.88 μM $AgNO_3$, and 0.94 μM $NaBH_4$, which was then allowed to sit in the dark at room temperature for 0.5 h to form AgNCs.

Analytical Procedures. Before use, the oligonucleotide NCB probe was refolded into a hairpin structure through heating to 95 °C for 3 min and then allowed to gradually cool down to room temperature to ensure the formation of a stem−loop DNA structure. Upon optimizing various conditions, a typical analytical procedure for this ratiometric fluorescence biosensor could be briefly described as follows: First, 20 μL of the DNA target with different concentrations was added to 15 μL of the NaAc solution (20 mM, pH 7.5) containing a 1.0 μM NCB probe. After incubation for 20 min at room temperature to enable sufficient hybridization of the target DNA and the NCB probe, the AgNCs were prepared by adding 10 μL of 18.8 μM $AgNO_3$ into the target/NCB probe reaction solution, followed by vigorously shaking for 30 s. Then, the mixture was incubated in the dark at 4 °C for 30 min. Subsequently, 10 μL of 9.4 μM freshly prepared $NaBH_4$ solution was added with vigorous shaking for another 30 s. The aqueous solution of $NaBH_4$ was prepared by dissolving $NaBH_4$ powder in ultrapure water and adding the required volume to the mixture within 30 s. After that, 45 μL of the NaAc solution was added to the mixture to a final volume of 100 μL. The resultant reaction mixture was kept in the dark at room temperature for 0.5 h to form AgNCs and was finally transferred into a quartz cuvette for fluorescence measurements.

RESULTS AND DISCUSSION

In the past decade, many efforts have been made in the oligonucleotide-stabilized AgNCs, and various DNA templates were explored to synthesize AgNCs. Among them, RNuS (5′-CACCGCTTTTGCCTTTTGGGGACGGATA-3′)[39] has been demonstrated to be an effective template to produce 15-atom AgNCs with an intense red emission at ∼670 nm (Figure 1C) and a fluorescence quantum yield of 75%, which could be excited by visible light (λ_{ex} = ∼610 nm) with a characteristically large Stoke's shift. In this work, we found that, as shown in Figure 1A,B, the RNuS consists of a GNuS (5′-TGCCTTTTGGGGACGGATA-3′), which was shown to generate green-emissive AgNCs[39] with a bright green fluorescence emission at ∼565 nm when excited at 500 nm (Figure 1E), and a 9-nt fragment (5′-CACCGCTTT-3′), which could not generated any emissive AgNCs (Figure 1D). In other words, the GNuS could be transformed to RNuS through the connection of a 9-nt fragment onto its 5′ terminal.

To better understand this template-transformation mechanism and to find a general rationale for designing template-transformation-based ratiometric NCBs for DNA sequence detection, a series of GNuS derivatives were designed through the sequential 5′ additions to GNuS base by base according to the sequence of the 9-nt fragment (5′-CACCGCTTT-3′). These studies have practical importance because the template sequence dictates the spectral properties of AgNCs.[40] Table S1 shows a series of DNA sequences of varying lengths, on the basis of the original RNuS sequence. Using the above sequences as hosts, the AgNC synthesis was carried out under the same conditions in the presence of Ag^+ through the reduction by $NaBH_4$. Figure 2 shows the fluorescence features of the obtained DNA-Ag solutions in the form of contour maps. The primary fluorescence peaks produced by the first three elongated derivatives with 20−22 nucleotides (i.e., 5′-$\underline{T}_n$GNuS-3′, n = 1, 2, 3, respectively) lie at the similar wavelengths with similar intensities (Figure 2A−C). Because the optical properties of few-atom AgNCs are sensitive to changes in the cluster size of just one atom and to the template sequence of just one base as well as to the cluster shape,[39] the lack of spectral

DOI: 10.1021/acsami.7b03198
ACS Appl. Mater. Interfaces 2017, 9, 13102−13110

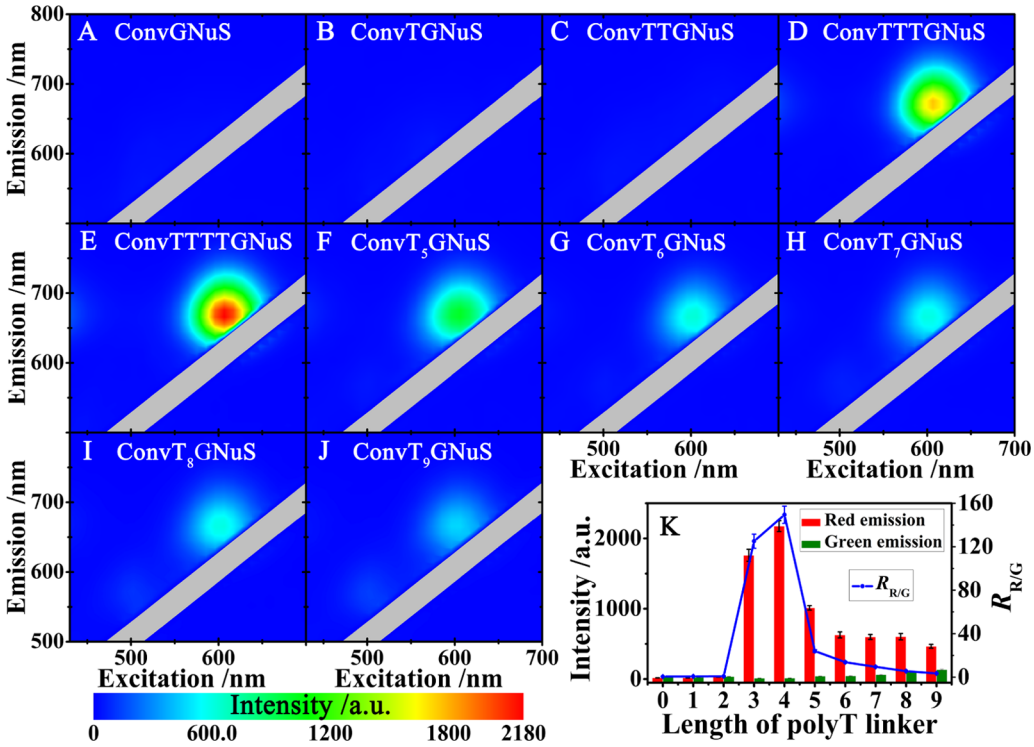

Figure 3. (A–J) Two-dimensional fluorescence contour maps of AgNCs stabilized by RNuSs with different T-linker lengths. (K) Bar plots of the emission peak intensities in A–J and the calculated $R_{R/G}$.

changes with 5′-T_n (n = 1, 2, 3) tails shows that the AgNC structures are essentially unaffected, which was presumably attributed to the fact that thymine has the weakest binding affinity for silver ions among the four nucleobases (interaction strength: C > G > A > T).[41] In contrast, the addition of only one C base (5′-CT_3GNuS, Figure 2D) dramatically declined the green fluorescence emission of GNuS, indicating that the generation of green-emissive AgNCs on this template is greatly inhibited. With the continuous elongation of 5′-CT_3GNuS-3′, the green fluorescence emission disappeared gradually (Figure 2D–G). However, no red fluorescence emission was observed until the eighth base was appended (5′-ACCGCT_3GNuS-3′, Figure 2H), and the red fluorescence emission of AgNCs obtained on 5′-CACCGCT_3GNuS-3′ increased remarkably (Figure 2I).

Results from the above experiments reflect that the bases in the 5′-CACCGC-3′ sequence directly contribute to the template transformation from GNuS to RNuS. Therefore, the 5′-CACCGC-3′ sequence acts as a template convertor (Conv) in this study, which is connected to the GNuS through the polyT linker (5′-TTT-3′). We further checked whether the length of the embedded polyT linker between the convertor and the GNuS could affect the template transformation (sequences in Table S2). Here, the fluorescence intensity ratio of red emission (λ_{ex} = 600 nm, λ_{em} = 670 nm) and green emission (λ_{ex} = 500 nm, λ_{em} = 565 nm), which is denoted as $R_{R/G}$, was used to estimate the template transformation efficiency. Obviously, the larger the $R_{R/G}$, the higher the template-transformation efficiency. As shown in Figure 3A–C, none of the 5′-ConvGNuS-3′, 5′-ConvTGNuS-3′, or 5′-ConvT_2GNuS-3′ sequence produced obvious fluorescence for excitation across the studied range. The $R_{R/G}$ for these three templates is 0.5274, 0.6834, and 0.8257, respectively (Figure 3K). When using 5′-ConvT_3GNuS-3′ as the scaffold for AgNC synthesis, an intense red fluorescence signal of AgNCs was detected (Figure 3D) with an $R_{R/G}$ of 125.1 (Figure 3K). To our surprise, the 5′-ConvT_4GNuS-3′ template yielded more efficient template transformation ($R_{R/G}$ = 149.4, Figure 3K) than the 5′-ConvT_3GNuS-3′ sequence due to its enhanced red emission intensity (Figure 3E), indicating that the 29-nt RNuS with the T_4 linker harbored a better binding site for the red fluorescence emissive AgNCs than the reported 5′-ConvT_3GNuS-3′ sequence. As evidenced by the gradually decreased red fluorescence emission intensity in Figure 3F–J, a longer polyT linker (5′-T_n-3′, n > 4) tended to deteriorate the cluster growth microenvironment for the red fluorescence emissive AgNCs. In contrast, accompanied by the rapid decrease of the red fluorescence emission intensity, the extent of green fluorescence emission was found to slowly increase with the further increase of the T-base number in the polyT linker (Figure 3F–J), which implies that the long distance between the convertor and the GNuS weakens the template transformation ability of the convertor sequence, resulting in low $R_{R/G}$ (Figure 3K). These fluorescence spectra demonstrated that appropriate proximity of the convertor to GNuS is necessary for the template transformation and suggested that the four-base polyT linker provided the highest $R_{R/G}$ and, thus, the optimal template transformation efficiency. Therefore, unless otherwise specified in this work, RNuS with a four-base polyT linker was selected as the nucleation sequence for red-emissive AgNCs.

On the basis of the above findings, we developed a new strategy to design NCBs with a ratiometric fluorescent response through artificially breaking the connection between the convertor and the GNuS. The schematic illustration of the proposed ratiometric NCB for label-free detection of the Hepatitis-A virus (HAV) gene, a proof-of-concept target in this work, is illustrated in Figure 4A. First, the RNuS was split into

DOI: 10.1021/acsami.7b03198
ACS Appl. Mater. Interfaces 2017, 9, 13102–13110

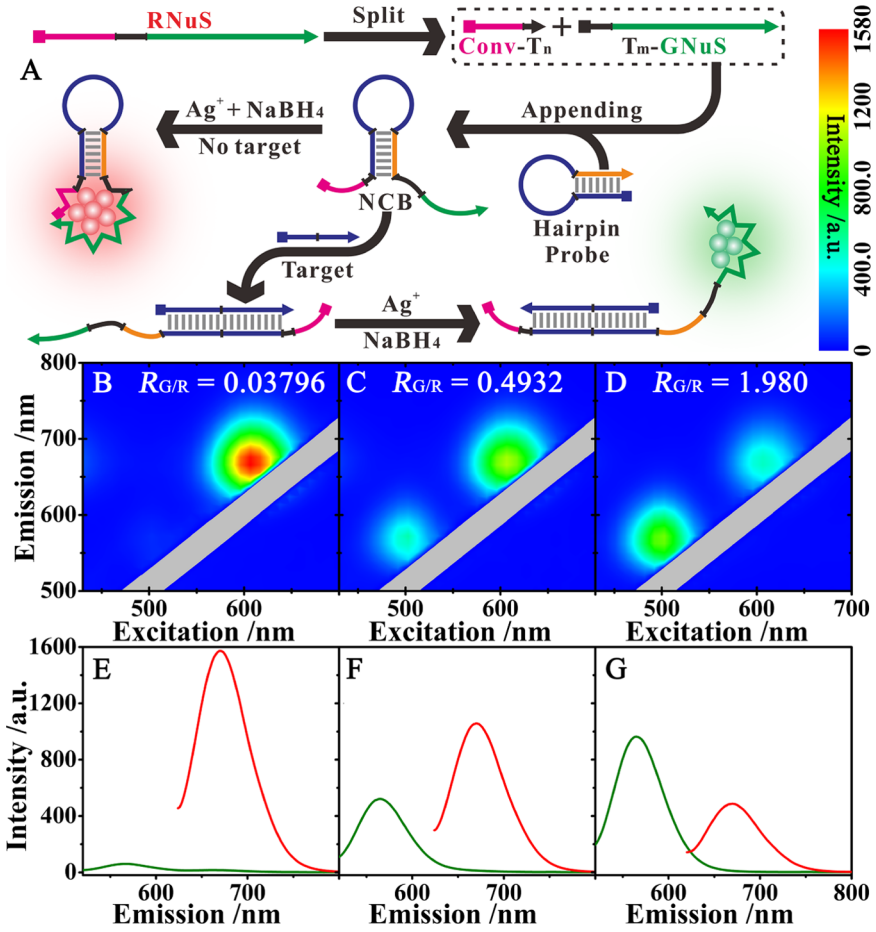

Figure 4. (A) Schematic illustration of the ratiometric NCB on the basis of the target-induced template transformation strategy. (B–D) Two-dimensional fluorescence contour maps and (E–G) fluorescence emission spectra of NCBs without (B) and with a 10 nM (C) and 100 nM (D) target. The excitation wavelength of the green line and the red line in (E)–(G) is 500 and 610 nm, respectively.

two portions with the cut site located on the T_4 linker, that is, 5′-ConvT-3′ and 5′-T_3GNuS-3′. Then, as shown in Figure 4A, the ratiometric NCB is constructed through appending the two portions, respectively, onto the 5′-terminus and 3′-terminus of a rationally designed hairpin probe for HAV. In the absence of the target HAV, the two portions will be in proximity upon the hybridization of the complementary stem to form an intact RNuS, which, similar to the original RNuS (Figure 1C), will facilitate the synthesis of red fluorescence emissive AgNCs. Upon the addition of the target HAV, as shown in Figure 4A, the NCB hybridizes with HAV by pairing to the whole loop and stem region, which opens the stem domain of the hairpin and allows the spatial and physical separation of the convertor from the GNuS, leading to the formation of green fluorescence emissive AgNCs on GNuS upon reduction in the presence of silver ions. Therefore, for this target-induced template-transformation strategy, an intense green fluorescence emission is expected when the target strand is present to induce the transformation of RNuS to GNuS, whereas the fluorescence emission should remain bright red when the target sequence is absent. Here, this red fluorescence intensity can be treated as the background, and the green one enhanced by the target can be regarded as the target signal. Figure 4B–D shows the fluorescence contour maps of the obtained DNA-Ag solutions, 0.5 h after the addition of Ag^+ to the above-mentioned NCB in the absence and presence of the target and reduction with $NaBH_4$. As shown in Figure 4B,E, however, contrary to original expectation, both red and green emissions were observed in the absence of the target strand, which can be attributed to the trace amount of unfolded NCB due to the incomplete hybridization or it could be due to the transient unraveling of the ends of the stem hybrid. With the addition of target HAV, the fluorescence of NCB at ∼670 nm decreases (Figure 4C,F), whereas the fluorescence at ∼565 nm increases, demonstrating that target HAV disturbs the formation of the red AgNC species fluorescing at the ∼670 nm emission peak but contributes to the production of the green species corresponding to the ∼565 nm emission peak. Importantly, the opposite fluorescence changes of two emitters with the increase of the target concentration (Figure 4D,G) further validated the template transformation on NCB. Moreover, the ratio of the signal to the background ($R_{G/R}$) varies considerably for different target concentrations (Figure 4B–D), suggesting that the proposed NCB is feasible for target HAV detection. Furthermore, compared with the contour map in Figure 1C,E, the AgNCs formed on such an NCB either in the absence or in the presence of the target strand exhibited the same fluorescence profiles (excitation and emission wavelengths) as that stabilized by the original RNuS or GNuS sequence, but they emit a lower fluorescence intensity. The reason why the overall fluorescence intensity is higher on the original RNuS/GNuS template versus NCB is not fully understood. One possible explanation could be that, admittedly, the hairpin regions of the NCB might also act as a template to support the

DOI: 10.1021/acsami.7b03198
ACS Appl. Mater. Interfaces 2017, 9, 13102–13110

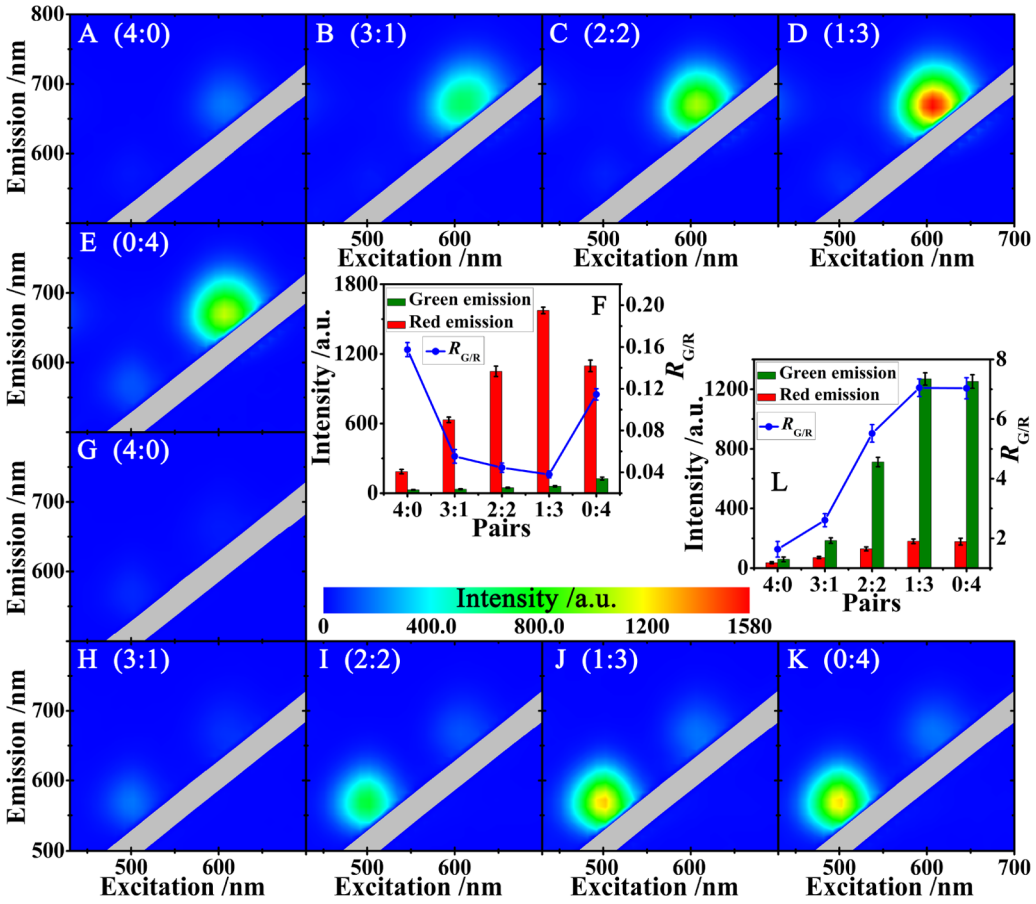

Figure 5. Two-dimensional fluorescence contour maps of NCBs attached with different split pairs in the absence (A–E) and presence (G–K) of a 500 nM target. Bar plots of the emission peak intensities in A–E (F) and G–K (L) and the calculated $R_{G/R}$.

formation of dark AgNCs, which influenced the original fluorescence emission of the RNuS- or GNuS-stabilized AgNCs on NCB.

Because our ratiometric fluorescent NCBs rely on the transformation of the AgNC scaffold induced by the target, it is of great importance to make sure that the change of the fluorescence emission is owing to the target-induced separation of the convertor and GNuS and to find out the optimal way to split the RNuS for template transformation. Thus, a series of control experiments were carried out in this study. First, to clarify that the fluorescent signals were derived from the attached RNuS or GNuS, the stem–loop sequence without the 5′-ConvT-3′ and 5′-T_3GNuS-3′ was tested as the template for the AgNC synthesis under the same conditions in the presence or absence of the target HAV sequence. The data obtained (Figure S1) clearly show that the hairpin structure without the 5′-ConvT-3′ and 5′-T_3GNuS-3′ overhangs could not guide the formation of fluorescent AgNCs. Both the fluorescence emission and the emission transformation, as detection signals proposed in our study, were derived only from the RNuS or GNuS sequence rather than the hairpin structure (Figure S1A), target sequence (Figure S1B), or their hybrid (Figure S1C). Second, we split the RNuS into two portions with the different cut sites located on the polyT linker, that is, 5′-ConvT_n-3′ and 5′-T_mGNuS-3′, $m + n = 4$. All five possible ways to split the RNuS are illustrated in Table S4. These five split pairs are named pair (n:m): for example, pair (0:4), pair (1:3), pair (2:2), pair (3:1), and pair (4:0). As shown in Figure S2, we noticed that the emission patterns of these split pairs in the absence and presence of the hairpin probe before and after target introduction are all similar to that of the GNuS-hosted AgNCs (Figure 1E), indicating that the convertor sequence (5′-ConvT_n-3′) had no significant effect on the fluorescence properties of 5′-T_mGNuS-3′ without the aid of the duplex stem regardless of the presence or absence of the hairpin probe and the target sequence, which further confirmed the importance of proximity on the template transformation. Finally, we tested all of the five split pairs attached on the hairpin probe as the template for AgNC synthesis under the same conditions. Figure 5 summarizes the fluorescence contour maps of these NCBs in the presence and absence of a 500 nM target HAV sequence. As both the red and green emission peaks varied in these NCBs, the $R_{G/R}$ of the different NCBs were compared. In the absence of a target, as the cut site approaches the convertor, that is, from pair (4:0) to pair (0:4) (Figure 5A–E), the red fluorescence emission of NCBs increased and reached a maximum value at pair (1:3), whereas the green fluorescence emission of NCBs (signal fluorescence) was low and remained nearly unchanged, leading to a dramatic reduction in the $R_{G/R}$ of pair (1:3) (Figure 5F). In the presence of a target, although both the red and the green fluorescence emissions increased as the cut site approached the convertor (Figure 5G–K), the green fluorescence emission increased more rapidly, which led to a high $R_{G/R}$ at pair (1:3) and pair (0:4) (Figure 5L). Therefore, upon close examination of the resulting spectra, we experimentally chose pair (1:3) for the construction of NCBs, which provides the lowest $R_{G/R}$ in the absence of a target and the highest $R_{G/R}$ in the presence of a target.

DOI: 10.1021/acsami.7b03198
ACS Appl. Mater. Interfaces 2017, 9, 13102–13110

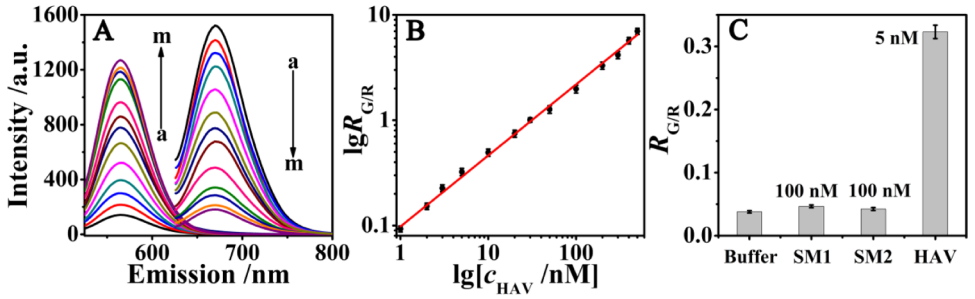

Figure 6. (A) Fluorescence responses of the proposed NCB to different concentrations of HAV (from a to m: 1.0, 2.0, 3.0, 5.0, 10, 20, 30, 50, 100, 200, 300, 400, and 500 nM). (B) The linear relationship of the logarithmic value of $R_{G/R}$ vs the logarithm of HAV concentration. (C) Selectivity of this ratiometric NCB.

On the basis of the above results, the proposed NCB was then applied as a ratiometric fluorescence nanoprobe for sensitive detection of HAV. As shown in Figure 6A, upon the addition of increased concentrations of HAV, the green emission intensity (I_G, at ~565 nm) of the NCBs is gradually restored, whereas the red one (I_R, at ~670 nm) decreases concomitantly, which demonstrated that the proposed NCB was a ratiometric fluorescence sensor for HAV. Accordingly, as can be seen in Figure 6B, the relative emission intensity ratio of green emission to red emission ($R_{G/R} = I_G/I_R$) is closely related to the amount of the target HAV and increases from 0.09281 to 6.996 along with the concentration of the target HAV over the dynamic concentration range from 1.0 to 500 nM, which formed the basis for the quantitative detection of target HAV. It can be clearly seen that the logarithmic (log) value of $R_{G/R}$ exhibited a good linear relationship with the logarithm of the target HAV concentration over the examined concentration profile, which can be represented by the linear regression equation, $\log R_{G/R} = 0.6747 \times \log[c_{HAV}\ (nM)] - 1.009$, with a correlation coefficient of 0.9975. Benefiting from the well-resolved dual emissions and the relatively large range of emission intensity ratios of $R_{G/R}$, the limit of detection is estimated to be 0.5 nM according to the 3σ IUPAC criteria, which is comparable to or even better than that of many other reported fluorescence biosensors. The detailed comparison of the proposed NCB-based ratiometric fluorescence biosensor with others was illustrated in Table S5. In addition, the data points in the calibration curve represent six independent measurements, which show the relative standard deviations (n = 6) ranging from 2.67 to 8.16% for the target HAV at various concentrations, indicating good reproducibility of the proposed NCB-based ratiometric fluorescence biosensor. Importantly, the NCBs retain the high sequence specificity that arises from the conformational constraint of the stem–loop structures.[42] We interrogated two targets carrying a single-nucleotide mismatch to investigate the sequence discrimination ability of the proposed NCB. The sequences of the mismatched DNA targets (SM1 and SM2) are shown in Table S3. As expected, the $R_{G/R}$ responses for the two single mismatched targets at the same condition were significantly lower than those of perfectly matched targets and are similar to those of the target-free reaction (Figure 6C), indicating a good selectivity of the proposed NCB. These data clearly suggest that NCB can not only recognize specific gene targets but also might be appropriate for more challenging applications such as allele discrimination.

To evaluate the feasibility of the proposed ratiometric NCB in practical sample analysis, such as human serum sample, first, it is important to challenge the proposed NCB in a higher salt concentration solution to test its salt tolerance. Figure S3 shows that no significant influence on the fluorescence features of the proposed NCB was observed in the absence or presence of the target HAV upon the addition of up to 80 mM $NaNO_3$ before AgNC synthesis. Then, a recovery test was performed by challenging the ratiometric NCB in spiked human serum samples, which was implemented through spiking different amounts of HAV into 1% diluted human serum. The assay results are summarized in Table 1, which shows that the calculated recoveries are in the range of 92.6–104.8% (n = 6). These obtained results demonstrated that the proposed ratiometric NCB shows a promise for HAV detection in practical applications with acceptable accuracy and reliability.

Table 1. Recovery Experiments for HAV-Spiked Human Serum Samples

samples	spiked (nM)	found (nM)	recovery (%)
sample 1	5.0	4.63 ± 0.4	92.6
sample 2	50	52.4 ± 3.5	104.8
sample 3	500	486 ± 15.7	97.2

CONCLUSIONS

In summary, the starting point of our design is that the splitting of RNuS at a specific site generates GNuS. The template-transformation mechanism was systematically investigated using a series of GNuS/RNuS derivatives. Experimental results showed that the connection of the 6-nt convertor to the 5′-end of the GNuS through a T_3 linker (5′-TTT-3′) would transform the GNuS to the RNuS. Importantly, we found that the RNuS derivative with a T_4 linker turns out to be, unexpectedly, an optimized RNuS in this study, having the strongest fluorescence intensity and, thus, providing the highest template transformation efficiency. To the best of our knowledge, this is the first attempt to explore an AgNC template-transformation strategy through sequence splitting or/and integrating. On the basis of the hybridization proximity mode, a ratiometric NCB has been developed by appending the split RNuS onto a rationally designed hairpin probe. We further explored various NCB designs and found that the most effective way to split the RNuS is 1:3 cutting on the polyT linker. The generation of green-emissive AgNCs after the binding of a target sequence to the NCB often comes with the decrease of red-emissive AgNCs. Therefore, this NCB could respond to the target sequence ratiometrically with remarkable emission ratio ($R_{G/R}$) changes, allowing sensitive detection of HAV down to 0.5 nM.

DOI: 10.1021/acsami.7b03198
ACS Appl. Mater. Interfaces 2017, 9, 13102–13110

More notably, the proposed NCB avoids both the strict selection and the complicated dual-labeling of the ideal fluorophore (donor)−quencher (acceptor) pair, endowing the probes design with more flexibility and low cost. Thus, we believe our findings would enable greater diversity of applications of DNA-hosted AgNCs and pave the grounds for designing new fluorescence biosensors.

■ ASSOCIATED CONTENT

Supporting Information

The Supporting Information is available free of charge on the ACS Publications website at DOI: 10.1021/acsami.7b03198.

Sequences of oligonucleotides; 2D fluorescence contour plots of control experiments; comparison of the present study with other fluorescence biosensors (PDF)

■ AUTHOR INFORMATION

Corresponding Author

*E-mail: lifeng@qust.edu.cn. Tel: +86-532-86080855.

ORCID

Feng Li: 0000-0002-3894-6139

Notes

The authors declare no competing financial interest.

■ ACKNOWLEDGMENTS

This work was financially supported by National Natural Science Foundation of China (31501570 and 21575074), Natural Science Foundation of Shandong Province, China (ZR2014BQ011), Basic Research Program of Qingdao (16-5-1-55-jch), Research Foundation for Distinguished Scholars of Qingdao Agricultural University (663-1115003 and 663-1113311), and the Special Foundation for Distinguished Taishan Scholar of Shandong Province (ts201511052).

■ REFERENCES

(1) Li, J.; Zhu, J.-J.; Xu, K. Fluorescent Metal Nanoclusters: From Synthesis to Applications. *TrAC, Trends Anal. Chem.* **2014**, *58*, 90−98.

(2) Zhang, L.; Wang, E. Metal Nanoclusters: New Fluorescent Probes for Sensors and Bioimaging. *Nano Today* **2014**, *9*, 132−157.

(3) Liu, J. DNA-Stabilized, Fluorescent, Metal Nanoclusters for Biosensor Development. *TrAC, Trends Anal. Chem.* **2014**, *58*, 99−111.

(4) Yuan, Z.; Chen, Y.-C.; Li, H.-W.; Chang, H.-T. Fluorescent Silver Nanoclusters Stabilized by DNA Scaffolds. *Chem. Commun.* **2014**, *50*, 9800−9815.

(5) Liu, Y.-Q.; Zhang, M.; Yin, B.-C.; Ye, B.-C. Attomolar Ultrasensitive Microrna Detection by DNA-Scaffolded Silver-Nanocluster Probe Based on Isothermal Amplification. *Anal. Chem.* **2012**, *84*, 5165−5169.

(6) Liu, X.; Wang, F.; Aizen, R.; Yehezkeli, O.; Willner, I. Graphene Oxide/Nucleic-Acid-Stabilized Silver Nanoclusters: Functional Hybrid Materials for Optical Aptamer Sensing and Multiplexed Analysis of Pathogenic DNAs. *J. Am. Chem. Soc.* **2013**, *135*, 11832−11839.

(7) Zhang, L.; Zhu, J.; Guo, S.; Li, T.; Li, J.; Wang, E. Photoinduced Electron Transfer of DNA/Ag Nanoclusters Modulated by G-Quadruplex/Hemin Complex for the Construction of Versatile Biosensors. *J. Am. Chem. Soc.* **2013**, *135*, 2403−2406.

(8) Qi, L.; Huo, Y.; Wang, H.; Zhang, J.; Dang, F.-Q.; Zhang, Z.-Q. Fluorescent DNA-Protected Silver Nanoclusters for Ligand−Hiv RNA Interaction Assay. *Anal. Chem.* **2015**, *87*, 11078−11083.

(9) Chen, J.; Ji, X.; Tinnefeld, P.; He, Z. Multifunctional Dumbbell-Shaped DNA-Templated Selective Formation of Fluorescent Silver Nanoclusters or Copper Nanoparticles for Sensitive Detection of Biomolecules. *ACS Appl. Mater. Interfaces* **2016**, *8*, 1786−1794.

(10) Ma, J.-L.; Yin, B.-C.; Wu, X.; Ye, B.-C. Copper-Mediated DNA-Scaffolded Silver Nanocluster on−Off Switch for Detection of Pyrophosphate and Alkaline Phosphatase. *Anal. Chem.* **2016**, *88*, 9219−9225.

(11) Ye, T.; Chen, J.; Liu, Y.; Ji, X.; Zhou, G.; He, Z. Periodic Fluorescent Silver Clusters Assembled by Rolling Circle Amplification and Their Sensor Application. *ACS Appl. Mater. Interfaces* **2014**, *6*, 16091−16096.

(12) Shen, C.; Xia, X.; Hu, S.; Yang, M.; Wang, J. Silver Nanoclusters-Based Fluorescence Assay of Protein Kinase Activity and Inhibition. *Anal. Chem.* **2015**, *87*, 693−698.

(13) Xiao, Y.; Shu, F.; Wong, K.-Y.; Liu, Z. Förster Resonance Energy Transfer-Based Biosensing Platform with Ultrasmall Silver Nanoclusters as Energy Acceptors. *Anal. Chem.* **2013**, *85*, 8493−8497.

(14) Li, J.; Wang, W.; Sun, D.; Chen, J.; Zhang, P.-H.; Zhang, J.-R.; Min, Q.; Zhu, J.-J. Aptamer-Functionalized Silver Nanoclusters-Mediated Cell Type-Specific Sirna Delivery and Tracking. *Chem. Sci.* **2013**, *4*, 3514−3521.

(15) Yin, J.; He, X.; Wang, K.; Xu, F.; Shangguan, J.; He, D.; Shi, H. Label-Free and Turn-on Aptamer Strategy for Cancer Cells Detection Based on a DNA−Silver Nanocluster Fluorescence Upon Recognition-Induced Hybridization. *Anal. Chem.* **2013**, *85*, 12011−12019.

(16) Li, J.; You, J.; Dai, Y.; Shi, M.; Han, C.; Xu, K. Gadolinium Oxide Nanoparticles and Aptamer-Functionalized Silver Nanoclusters-Based Multimodal Molecular Imaging Nanoprobe for Optical/Magnetic Resonance Cancer Cell Imaging. *Anal. Chem.* **2014**, *86*, 11306−11311.

(17) Li, J.; Zhong, X.; Cheng, F.; Zhang, J.-R.; Jiang, L.-P.; Zhu, J.-J. One-Pot Synthesis of Aptamer-Functionalized Silver Nanoclusters for Cell-Type-Specific Imaging. *Anal. Chem.* **2012**, *84*, 4140−4146.

(18) Jiang, H.; Xu, G.; Sun, Y.; Zheng, W.; Zhu, X.; Wang, B.; Zhang, X.; Wang, G. A "Turn-on" Silver Nanocluster Based Fluorescent Sensor for Folate Receptor Detection and Cancer Cell Imaging under Visual Analysis. *Chem. Commun.* **2015**, *51*, 11810−11813.

(19) Tao, Y.; Li, Z.; Ju, E.; Ren, J.; Qu, X. One-Step DNA-Programmed Growth of Cpg Conjugated Silver Nanoclusters: A Potential Platform for Simultaneous Enhanced Immune Response and Cell Imaging. *Chem. Commun.* **2013**, *49*, 6918−6920.

(20) Li, T.; Zhang, L.; Ai, J.; Dong, S.; Wang, E. Ion-Tuned DNA/Ag Fluorescent Nanoclusters as Versatile Logic Device. *ACS Nano* **2011**, *5*, 6334−6338.

(21) Huang, Z.; Tao, Y.; Pu, F.; Ren, J.; Qu, X. Versatile Logic Devices Based on Programmable DNA-Regulated Silver-Nanocluster Signal Transducers. *Chem. − Eur. J.* **2012**, *18*, 6663−6669.

(22) Zhou, Z.; Liu, Y.; Dong, S. DNA-Templated Ag Nanoclusters as Signal Transducers for a Label-Free and Resettable Keypad Lock. *Chem. Commun.* **2013**, *49*, 3107−3109.

(23) Yeh, H.-C.; Sharma, J.; Han, J. J.; Martinez, J. S.; Werner, J. H. A DNA−Silver Nanocluster Probe That Fluoresces Upon Hybridization. *Nano Lett.* **2010**, *10*, 3106−3110.

(24) Li, J.; Zhong, X.; Zhang, H.; Le, X. C.; Zhu, J.-J. Binding-Induced Fluorescence Turn-on Assay Using Aptamer-Functionalized Silver Nanocluster DNA Probes. *Anal. Chem.* **2012**, *84*, 5170−5174.

(25) Juul, S.; Obliosca, J. M.; Liu, C.; Liu, Y.-L.; Chen, Y.-A.; Imphean, D. M.; Knudsen, B. R.; Ho, Y.-P.; Leong, K. W.; Yeh, H.-C. Nanocluster Beacons as Reporter Probes in Rolling Circle Enhanced Enzyme Activity Detection. *Nanoscale* **2015**, *7*, 8332−8337.

(26) Xu, M.; Gao, Z.; Wei, Q.; Chen, G.; Tang, D. Label-Free Hairpin DNA-Scaffolded Silver Nanoclusters for Fluorescent Detection of Hg2+ Using Exonuclease Iii-Assisted Target Recycling Amplification. *Biosens. Bioelectron.* **2016**, *79*, 411−415.

(27) Liu, G.; Li, J.; Feng, D.-Q.; Zhu, J.-J.; Wang, W. Silver Nanoclusters Beacon as Stimuli-Responsive Versatile Platform for Multiplex DNAs Detection and Aptamer−Substrate Complexes Sensing. *Anal. Chem.* **2017**, *89*, 1002−1008.

(28) Gong, L.; Kuai, H.; Ren, S.; Zhao, X.-H.; Huan, S.-Y.; Zhang, X.-B.; Tan, W. Ag Nanocluster-Based Label-Free Catalytic and Molecular Beacons for Amplified Biosensing. *Chem. Commun.* **2015**, *51*, 12095−12098.

DOI: 10.1021/acsami.7b03198
ACS Appl. Mater. Interfaces 2017, 9, 13102−13110

(29) Xiao, Y.; Wu, Z.; Wong, K.-Y.; Liu, Z. Hairpin DNA Probes Based on Target-Induced in Situ Generation of Luminescent Silver Nanoclusters. *Chem. Commun.* **2014**, *50*, 4849−4852.
(30) Chen, Y.-A.; Obliosca, J. M.; Liu, Y.-L.; Liu, C.; Gwozdz, M. L.; Yeh, H.-C. Nanocluster Beacons Enable Detection of a Single N6-Methyladenine. *J. Am. Chem. Soc.* **2015**, *137*, 10476−10479.
(31) Zhang, Y.; Zhu, C.; Zhang, L.; Tan, C.; Yang, J.; Chen, B.; Wang, L.; Zhang, H. DNA-Templated Silver Nanoclusters for Multiplexed Fluorescent DNA Detection. *Small* **2015**, *11*, 1385−1389.
(32) Zhang, J.; Li, C.; Zhi, X.; Ramón, G. A.; Liu, Y.; Zhang, C.; Pan, F.; Cui, D. Hairpin DNA-Templated Silver Nanoclusters as Novel Beacons in Strand Displacement Amplification for Microrna Detection. *Anal. Chem.* **2016**, *88*, 1294−1302.
(33) Liu, J.; Lu, Y.; Feng, L.; Wang, S.; Zhang, S.; Zhu, X.; Sheng, L.; Zhang, S.; Zhang, X. Pinpoint the Positions of Single Nucleotide Polymorphisms by a Nanocluster Dimer. *Anal. Chem.* **2017**, *89*, 2622−2627.
(34) Lee, M. H.; Kim, J. S.; Sessler, J. L. Small Molecule-Based Ratiometric Fluorescence Probes for Cations, Anions, and Biomolecules. *Chem. Soc. Rev.* **2015**, *44*, 4185−4191.
(35) Wang, S.; Li, N.; Pan, W.; Tang, B. Advances in Functional Fluorescent and Luminescent Probes for Imaging Intracellular Small-Molecule Reactive Species. *TrAC, Trends Anal. Chem.* **2012**, *39*, 3−37.
(36) Liu, L.; Yang, Q.; Lei, J.; Xu, N.; Ju, H. DNA-Regulated Silver Nanoclusters for Label-Free Ratiometric Fluorescence Detection of DNA. *Chem. Commun.* **2014**, *50*, 13698−13701.
(37) Ge, L.; Wang, W.; Sun, X.; Hou, T.; Li, F. Affinity-Mediated Homogeneous Electrochemical Aptasensor on a Graphene Platform for Ultrasensitive Biomolecule Detection Via Exonuclease-Assisted Target-Analog Recycling Amplification. *Anal. Chem.* **2016**, *88*, 2212−2219.
(38) Liu, X.; Li, W.; Hou, T.; Dong, S.; Yu, G.; Li, F. Homogeneous Electrochemical Strategy for Human Telomerase Activity Assay at Single-Cell Level Based on T7 Exonuclease-Aided Target Recycling Amplification. *Anal. Chem.* **2015**, *87*, 4030−4036.
(39) Schultz, D.; Gardner, K.; Oemrawsingh, S. S. R.; Markešević, N.; Olsson, K.; Debord, M.; Bouwmeester, D.; Gwinn, E. Evidence for Rod-Shaped DNA-Stabilized Silver Nanocluster Emitters. *Adv. Mater.* **2013**, *25*, 2797−2803.
(40) Petty, J. T.; Fan, C.; Story, S. P.; Sengupta, B.; Sartin, M.; Hsiang, J.-C.; Perry, J. W.; Dickson, R. M. Optically Enhanced, near-IR, Silver Cluster Emission Altered by Single Base Changes in the DNA Template. *J. Phys. Chem. B* **2011**, *115*, 7996−8003.
(41) Shukla, S.; Sastry, M. Probing Differential Ag+-Nucleobase Interactions with Isothermal Titration Calorimetry (Itc): Towards Patterned DNA Metallization. *Nanoscale* **2009**, *1*, 122−127.
(42) Bonnet, G.; Tyagi, S.; Libchaber, A.; Kramer, F. R. Thermodynamic Basis of the Enhanced Specificity of Structured DNA Probes. *Proc. Natl. Acad. Sci. U.S.A.* **1999**, *96*, 6171−6176.

DOI: 10.1021/acsami.7b03198
ACS Appl. Mater. Interfaces 2017, 9, 13102−13110